Rapid determination of geographical authenticity and pungency intensity of the red Sichuan pepper (Zanthoxylum bungeanum) using differential pulse voltammetry and machine learning algorithms

Rapid determination of geographical authenticity and pungency intensity of the red Sichuan Pepper (*Zanthoxylum bungeanum*) using differential pulse voltammetry and machine learning algorithms

Di Zhang[1]; Zitao Lin[1]; Lilei Xuan[1]; Minmin Lu[1]; Bolin Shi[2*]; Jiyong Shi[1]; Fatao He[3]; Maurizio Battino[4,5]; Lei Zhao[2]; Xiaobo Zou[1]

1. School of Food and Biological Engineering, Jiangsu University, Zhenjiang, 212013, China

2. Food and Agriculture Standardization Institute, China National Institute of Standardization, Beijing, 102200, China

3. Jinan Fruit Research Institute, China Federation of Supply and Marketing Co-operatives, Jinan, Shandong, 250200, China

4. International Research Center for Food Nutrition and Safety, Jiangsu University, Zhenjiang, 212013, China

5. Department of Clinical Sciences, Faculty of Medicine, Polytechnic University of Marche, Ancona, Italy

* Corresponding Authors

Abstract

The development of an analytical method for assessing pungency intensity and determining geographical origins is crucial for evaluating the quality of visually similar Zanthoxylum bungeanum pericarp (PZB). This study analyzed 210 PZB samples from 14 origins across China, focusing on origin adulteration identification and pungency intensity using a combination of differential pulse voltammetry (DPV) and machine learning algorithms. The artificial neural network (ANN) and K-nearest neighbor (KNN) algorithms provided the highest accuracy in origin identification (100%) and adulteration detection (97.9%) respectively. Moreover, the ANN excelled in predicting pungency intensity (R^2 = 0.918). Assessment via feature importance analysis of DPV features revealed that segments of polyphenols (0.34-0.52V and 1.0-1.2V) and alkylamides (1.0-1.2V) contributed significantly to the PZB pungency intensity. These findings highlight the potential of DPV as a reliable method for assessing the quality of PZB, and offer a promising solution for ensuring the geographical authenticity of this important crop.

Keywords: Sichuan pepper; differential pulse voltammetry; origin; adulteration; pungency intensity

1 Introduction

Sichuan pepper (‘huajiao’ in Chinese, and the pericarp of *Zanthoxylum bungeanum* (PZB)), is a popular pungent condiment used widely in Asian cuisine. It is characterized by its distinctive tingling and numbing taste sensation, as well as its impressive aroma (Zhang et al., 2021). As Asian cuisine has gained popularity worldwide, the demand for Sichuan pepper has increased rapidly to the extent that PZB is now the largest cultivated woody spice crop globally, with more than one million hectares of plantations in China (Hu et al., 2023).

Effective assessments of PZB production place and pungency intensity are critical to the success of its commercial trade and deep processing, respectively. Discrepancies in *Zanthoxylum bungeanum* growing areas naturally yield PZB with differences in qualities such as aroma, numbing taste, and appearance. Origin is regarded as the main basis on which the purchase price of PZB is judged (Feng et al., 2022; Li et al., 2020). Unfortunately, driven by economic competition, the issue of geographical authenticity has become problematic in PZB trade, involving prevalent mislabeling and adulteration. PZB adulteration includes mainly the mixing of PZB from high-quality origins with similar lower-quality counterparts. However, the verification of PZB geographical authenticity can be challenging, even for professionals, since the crops are so similar in appearance. Although high-performance liquid chromatography (HPLC) fingerprint spectrometry and headspace solid-phase microextraction–gas chromatography-mass spectrometry (HS-SPME-GC-

MS) have proven to be effective in accurately determining origin authenticity (Feng et al., 2022; Ke et al., 2018), the lack of portability and the complex operations involved in these procedures make them inconvenient for on-the-go detection during business transactions.

Pungency intensity, an important indicator of PZB quality during processing, is primarily attributed to specific alkylamides, such as sanshools, hydroxyl-sanshools, bungeanool and isobungeanool (Artaria et al., 2011). Currently, the assessment of PZB pungency relies heavily on the subjective judgments of experts, but this approach requires sensory training and is limited by taste fatigue in large-scale test samples. On the other hand, current pungency intensity detection methods, which measure the content of alkylamide substances in PZB, do not accurately reflect the human sensory experience because the intensity is not dependent solely on the content of alkylamides but also their compositions (Feng et al., 2023). Alkylamides exhibit varying pungency intensities due to their structural differences (Kumar et al., 2014; Sugai et al., 2005). Furthermore, the sensory perception of the numbing taste can be influenced by other ingredients in the food matrix (Zhang et al., 2023), making it difficult to obtain reliable evaluation results solely through the measurement of specific alkylamide contents.

From the above analysis, it is clear that there is a demand for a high-precision and portable method to address the challenges posed by PZB origin identification as well as for the measurement of its pungency intensity. Recently, an electrochemical

78 instrument-based method, differential pulse voltammetry (DPV), has emerged as a
79 sensitive and selective tool in food quality evaluation (Marx, 2023). In our previous
80 research, it was found that DPV was able to yield voltammetric signals for the
81 polyphenols and alkylamides in PZB (Sun et al., 2020), thus presenting the potential
82 for distinguishing quality in different PZB. However, it emerged that there is obvious
83 interference among the signals derived from different ingredients, which hinders the
84 quantitative distinction between the quality characteristics of various PZB (Sun et al.,
85 2020a). Numerous studies have explored the use of specialized materials for electrode
86 modification, aimed at augmenting the selectivity and signal intensity of
87 electrochemical sensors (Ghoreishi et al., 2014; Valian et al., 2020). It has also been
88 reported that the fusion of machine learning and electrochemical detection can
89 provide an alternative approach that is able to compensate for limitations in the
90 traditional electrochemical method because it is superior in extracting meaningful
91 insights from complicated signals. Machine learning approach has been, thus, gaining
92 prominence in food quality monitoring (Shi et al., 2021; Yang et al., 2021; Berghian-
93 Grosan & Magdas, 2020; Karadağ et al., 2020).

94 The present study aimed to develop a rapid and accurate detection method for
95 both the geographical authenticity and pungency intensity of PZB via a combination
96 of DPV and machine learning algorithms. First, DP voltammograms of 210 PZB
97 samples from 14 origins across China were collected. Then, four algorithms, namely
98 support vector machine (SVM), KNN, ANN, and eXtreme gradient boosting (XGB),

were tested in the optimization of prediction models for origin, geographical authenticity and pungency intensity. In addition, the principles of origin differentiation and pungency intensity quantification in the proposed method were presented. To the best of our knowledge, this is the first time that voltammetry has been combined with deep learning technology to predict the quality of PZB. Furthermore, this study offers a promising approach for the development of PZB quality assessment instrumentation.

2 Materials and methods

2.1 Reagents

Purified hydroxyl-α-sanshool (α-SOH), hydroxyl-β-sanshool (β-SOH) and hydroxyl-γ-sanshool (γ-SOH) were purchased from the Maidesheng Chroma-Biotechnology Co., Ltd., China (HPLC purity ≥ 98.00%). Quercetin was purchased from Sigma-Aldrich (St. Louis, MO, USA). Ethanol (food grade) was purchased from Binzhou Guanglian Biochemical Co., Ltd. (Binzhou, China). Spring water was purchased from Wahaha Group Co. (Hangzhou, China). The essential oil of PZB was purchased from Hebei Runbu Biotechnology Co., Ltd. (Shijiazhuang, China). 1 mm, 0.5 mm and 0.03 mm alumina was purchased from Baird Material Technology Co., Ltd. (Suzhou, China). All other chemicals were of analytical grade and purchased from Sinopharm Chemical Reagent Co., Ltd. (Shanghai, China).

2.2 Collection of PZB samples

To ensure representativeness and authenticity, PZB samples were collected from

markets in 14 different significant PZB cultivation areas across China. A total of 15 batches were obtained from each origin, resulting in a collection of 210 samples from six provinces, namely Gansu (S1, S2, S3 and S4), Hebei (S5), Shandong (S6 and S7), Shaanxi (S8 and S9), Shanxi (S10) and Sichuan (S11, S12, S13 and S14). Samples S1, S2 and S3 were all from different subordinate counties in Tianshui, Gansu Province, while S4 was from another Gansu city, Linxia. These four PZB are known to have high pungency intensity, and a high yield of large fruit, so their prices are generally relatively moderate. The quality of S5-S8 is not as good as that of S1-S4 and, consequently, these PZB tend to be cheaper. S11-S14 were from subordinate counties and cities in Sichuan. Among them, S13 (from Sichuan Hanyuan) and S14 (from Sichuan Maowen) were the most expensive of all the samples because of their strong pungency, rich aroma and low yield. Detailed information of these samples is provided in Fig.1 and Table S1.

2.3 Adulterated samples of PZB

In the current market, S13 and S14 are considered the highest quality among this study's PZB samples, commanding prices that are more than double those of other PZB cultivars. Consequently, these two samples have become prime targets for fraud, often sold with other PZB varieties of lower quality mixed into the marketed product.

In this study, to mimic this fraudulent process, diverse adulterated PZB were formulated, with 12 blended combinations of S13 and S14 mixed respectively with six adulterants (S7 to S12). From each, five samples with different levels of

adulteration (20%, 35%, 50%, 65% and 80%, w/w) were prepared and, from each adulteration level in each combination, 10 adulterated PZB samples were prepared, resulting in a final total of 600 mixed samples. To ensure equilibrium between positive and negative samples during the training of the fraud identification model, a strategy was employed to augment the available data. This involved a randomized selection from the original 15 batches of S13 and S14 samples. By combining distinct batches from the same origin, new batches were formed, thus expanding the pool to encompass 60 batches for both the S13 and S14 samples. Importantly, these augmented batches were utilized exclusively for training the adulteration identification model.

2.4 Preparation of PZB extract and ingredient solutions for DPV analysis

2.4.1 PZB extract solutions

In all, there were 210 PZB authentic samples from 14 origins and 600 adulterated PZB samples comprising 12 combinations at five different levels of adulteration each. The PZB samples were first ground into powder using a smashing machine and then filtered through a 20-mesh screen. Subsequently, 5 g of PZB powder was mixed with 75 mL of absolute ethanol in a brown flask. The mixture was sonicated in an ultrasound bath (Shanghai Sonic Ultrasonic Instrument Ltd., China) for 20 min and then centrifuged at 2000 rpm for 5 min using a centrifuge (Kaida Centrifuge Ltd., China) and the supernatant was collected. To maintain consistency, the supernatants were adjusted to a volume of 200 mL with ethanol and stored at -18 ℃ prior to

voltametric analysis and sensory analysis.

2.4.2 Isolation of polyphenol fraction from PZB

Isolated polyphenol fractions (IPF) were prepared to analyze the electrochemical characteristics of the polyphenols in PZB. The preparative HPLC system (Beijing Separation Technology Ltd., China) was comprised of two SP-5030 preparative high-pressure infusion pumps, a UV/Vis detector, a fraction collector and an EasyChrom chromatography workstation. The chromatographic column was Sepax HP-C18 (10.0 mm × 250 mm, Sum) (Sepax Technologies Inc., China). The gradient elution method involved water as phase A and methanol as phase B, and followed sequential steps: 10% to 80% (B) within 0 to 20 min; transitioning from 80% to 90% (B) between 20 to 40 min; and, finally, 90% to 10% (B) in the final 10 min. The flow rate was set at 3.76 mL/min, the column temperature was maintained at 25℃, and the UV detector was set to measure absorbance at a wavelength of 290 nm. The S14 extracts were passed through a 0.22 um filter before 1 mL was injected into the preparative HPLC system. The retention of the polyphenol fractions ranged from 25 min to 33 min. The effluent fractions were collected and concentrated via rotary evaporation, followed by lyophilization, after which the lyophilized powder was dissolved into ethanol (30 g/L) for further use.

2.4.3 SOH and quercetin standard solutions

Stock solutions of purified α-SOH, β-SOH and γ-SOH standards were prepared in ethanol at concentrations of 10 g/L, 20 g/L, 30 g/L, 40 g/L and 50 g/L. The

pungency intensities of these SOH were calibrated using Scoville Pungency Units (SPU). Zhang et al. (2019) provided SPU values for pure α-SOH, β-SOH and γ-SOH, which were recorded as 23,100 SPU, 48,600 SPU and 27,800 SPU, respectively, and the SPU of a sample is inversely proportional to its dilution multiple (GB/T 38495, 2020). The SPU values of different concentrations of SOH solutions were converted accordingly, as shown in Table S2. Additionally, the quercetin standard solution was prepared at a concentration of 30 g/L.

2.5 DPV analysis

The DP voltammograms of the PZB extracts, IPF, SOHs and quercetin were recorded via a CHI660D electrochemical workstation (Shanghai CH Instruments, China). A three-electrode system was established, which consisted of a reference electrode (Ag/AgCl immersed in saturated KCl solution, Shanghai CH Instruments, China), a counter electrode (platinum wire, Shanghai CH Instruments, China), and a working electrode (glassy carbon electrode (GCE) , Shanghai CH Instruments, China), which first underwent a polishing process using 1 mm, 0.5 mm and 0.03 mm alumina slurry in sequence, followed by rinsing with distilled water. Thereafter, the GCE was sonicated successively in absolute ethanol and deionized water for 5 min to eliminate residual alumina particles. The three-electrode system was assembled in the cell for each DPV scanning. The polishing process was repeated after every scanning cycle.

After electrochemical cleaning of the GCE, A 0.5 mL sample solution was added to a 10 mL cell containing 9.5 mL supporting electrolyte comprised of 0.1 M

phosphate buffer solutions (PBS, pH=6.8), and the DP voltammogram was then recorded (Vilas-Boas et al., 2019). DPV parameters were set as follows: initial potential of -0.2 V; final potential of 1.4 V; potential step of 4 mV; amplitude of 0.05 V; pulse width of 0.05 s; sampling width of 0.0167 s; pulse period of 0.5 s; and quiet time of 2 s. Each sample was scanned three times, and the average value was taken.

2.6 Sensory analysis

Sensory analysis data on the pungency intensity of PZB was obtained from the China National Institute of Standardization. The study involved 15 trained sensory evaluators, aged between 22 and 30 years, with more than 200 hours of collective evaluation experience. In accordance with ethical guidelines, the informed consent of all participants on the sensory taste panel was obtained prior to their participation in the study. The general Labeled Magnitude Scale (gLMS), as described by Zhang et al. (2018), was employed as the method of sensory analysis.

To create reference samples of PZB pungency intensity, exactly 2 g PZB essential oil was dissolved in 20 mL of ethanol. The solution was heated in a water bath at 60℃ for 10 min, to which 20 mL of 70℃ water was then added. After being left to cool to room temperature, the solution was diluted to a total volume of 1 L with purified water. This stock solution was then progressively diluted with spring water, with the dilutions selected to cover a range of pungency intensities, as determined by sensory analysis. The gLMS values of the pungent reference samples were defined as 1.38 (barely detectable), 5.75 (weak), 16.22 (moderate), 33.11 (strong), 50.12 (very

strong) or 95.5 (strongest imaginable sensation of any kind). Concentrations of the reference system for different pungency intensities are listed in Table S3. The evaluators underwent training with semantic reference samples corresponding to the different scale values until they had effectively grasped the semantic descriptors and their associated pungency intensity values for the different reference samples.

The evaluators were tasked with performing sensory assessments of the 210 authentic PZB samples. During each assessment, the evaluators were instructed to sip 20 mL of the PZB extract, hold the liquid in their mouths for 40 sec and then spit out the sample. Subsequently, the evaluators were provided with the reference sample and asked to assign a relative value to the perceived pungency intensity of the tested sample. The evaluators used a scale that aligned with the pungency intensity description semantics depicted in Table S3. Each PZB sample was evaluated in three rounds, with the samples presented in a random and balanced order. The sensory analysis results for each evaluator were derived from the average of these three rounds of evaluations.

2.7 Data analysis

The analysis of data in this study was carried out using Python v3.9 programming language and Jupyter Notebook v6.4.5. Various packages such as NumPy v1.22.3, pandas v1.3.4, Matplotlib v3.4.3, SciPy v1.7.1, scikit-learn v1.0.2, PyTorch v1.10.0 and AutoGluon (Erickson et al., 2020) were utilized to develop models and perform data analysis. The data for the building model and source code

can be obtained at https://github.com/zt5544/pepper-detection-by-dpv.git.

2.7.1 Pre-processing

Pre-processing techniques offer several benefits, including the enhancement of accuracy and performance in machine learning models, the reduction of overfitting, and improvement of generalization to new data (Oliveri et al., 2019). Appropriate pre-processing can also mitigate issues such as bias and noise in the data, leading to more reliable and accurate results. Thus, careful pre-processing is essential for obtaining optimal model performance. To improve the quality of data, we have adopted a series of pre-processing methods, which we utilized to enhance the accuracy and reliability of our analysis. Specifically, we employed Savitzky-Golay smoothing (SG-S) to smooth out noise in the data (Press & Teukolsky, 1990). Moreover, we utilized standard normal variable transformation (SNV), which normalizes the data to mitigate issues such as bias (Barnes et al., 1989). This techniques are frequently utilized in spectral analysis and have proven to be effective in improving the analysis of one-dimensional electrochemical curves (Peris-Díaz & Krężel, 2021). To ensure all features were treated with equal importance in the model training process, we applied StandardScaler. StandardScaler scales data to a mean of 0 and a standard deviation of 1. This pre-processing techniques are commonly used to normalize data and ensure the provision of equal attention to all features in the model training process (Raju et al., 2020). The data was transformed by above pre-processing methods in sequence before being input into the models.

2.7.2 Dataset construction and description

Three distinct datasets were employed in the construction of machine learning models for the origin identification, adulteration identification and pungency intensity prediction of PZB. The process by which these datasets were established is illustrated in Fig. 2.

Dataset 1 was comprised of 210 DP voltammograms (15 different origins (S1-S14), each with 15 batches, totaling 210) of the PZB samples, further segmented into 14 categories, based on their origins.

Dataset 2 was designed specifically for adulteration and fraud identification purposes. It encompassed a total of 720 DPV curves of the PZB samples (60 batches each of S13 and S14; 10 batches each of adulterated samples mixed with S13, S14 and S6-S12 in five different proportions), labeled as either adulterated or non-adulterated. There were a total of 120 positive samples and 600 negative samples in this dataset, with 120 samples for each adulteration level amongst the negative samples. When training the model on this dataset, only one level of adulteration was used for negative sample data to ensure data balance.

Dataset 3 consisted of 210 DP voltammograms of the PZB samples (15 different origins (S1-S14), each with 15 batches, totaling 210), accompanied by their corresponding pungency intensity values. These pungency intensity values were obtained through the sensory evaluation results provided by the 15 panelists.

2.7.3 Origin differentiation model

Dataset 1 was tailored to determine the origin of each PZB sample. To visualize and illuminate the task of origin classification, principal component analysis (PCA) and linear discriminant analysis (LDA) algorithms were employed. PCA is a multivariate statistical analysis technique used to determine several principal component factors to represent the complex variables in an original sample. This facilitates the evaluation of regularity and differences between samples based on their contribution rates of principal component factors (Greener et al., 2022a). LDA is a statistical method used to find the linear combination of features that can best distinguish between two or more objects by minimizing intra-group variance and maximizing inter-group variance, thereby enhancing differentiation between the groups (Anowar et al., 2021)

Dataset 1 was divided into two sets at a ratio of 8:2, with 168 samples used for model training and optimization, and the remaining 42 samples used for testing. The pre-processing methods outlined in Section 2.8.1 were applied individually and in combinations. The endeavor encompassed the employment of the four distinct machine learning algorithms, namely KNN, SVM, ANN and XGB, all underpinned by k-fold cross-validation to construct robust models.

The methodology of k-fold cross-validation involves segmenting the training dataset into three equitably sized subsets or ‘folds’. This cyclic procedure is iterated thrice, with one-fold serving as an autonomous calibration set, while the remaining two are amalgamated to construct the training set. In essence, the model undergoes

training with two of the folds and is subsequently evaluated with the third, with the roles of training and testing sets interchanging dynamically in each iteration.

Optimization of the hyperparameters of each algorithm was executed via the grid search method. The optimizable hyperparameters encompassed the following diverse facets for each model: the number of neighbors (n_neighbors) for, weights, leaf_size, minkowski power parameter (p), algorithm used to compute the nearest neighbors (algorithm) for KNN; kernel function (kernel), cost (c) for SVM; learning rate, use batch normalization, dropout probability (dropout_prob), number of layers (num_layers), hidden layer size (hidden_size), weight decay, learning rate decay (gamma), L1 regularization coefficient (alpha) for ANN; number of estimators (n_estimators), learning rate, maximum depth of tree (max_depth), minimum child weight, L1 and L2 regularization terms (reg_alpha & reg_lambda) and minimum loss reduction required to make a further partition on a leaf node of the tree (gamma) for XGB. The search ranges for these hyperparameters are meticulously detailed in Table S4. Model performances were assessed using accuracy and precision, and the optimal algorithm and hyperparameter combination were selected for the optimal origin differentiation model. The performance of the model is measured by the accuracy and log loss.

2.7.4 Adulteration identification model

Dataset 2 was designed for the purpose of identifying adulteration. In order to ensure the balance of the dataset, each training session selected a combination of

negative and positive samples with different levels of adulteration for model training. A total of 5 models with different levels of adulteration were trained. The ratio of the training set to the test set is 8:2. The model optimization strategy is the same as the origin differentiation task including data preprocessing, three-fold cross-validation and grid search but the model performances were evaluated by accuracy, precision, recall, and area under the curve (AUC).

2.7.5 Pungency intensity evaluation model

For the pungency intensity evaluation model, Dataset 3 was divided into two sets, reserving 20% of the data (42 samples) for testing purposes, while the remaining 80% (168 samples) were designated for model training and optimization. We employed four distinct machine learning algorithms: KNN, SVM, ANN, and XGB for regression. Data preprocessing, three-fold cross-validation and grid search also be used. For this task, we used the same hyperparameter search range as the previous two tasks. To evaluate the pungency intensity evaluation model, we utilized two common regression metrics: R^2 (coefficient of determination) and RMSE (root mean square error). R^2 assesses the proportion of variance in the dependent variable (sensory analysis values) that is predictable from the independent variables (DP voltammograms), while RMSE quantifies the model's prediction error.

Upon identifying the most suitable model, we proceed to employ it in the calculation of feature importance. By quantifying the significance of various features within the curve data, the influence of DPV curve attributes on the pungency intensity

of PZB was assessed.

3 Results and discussion

3.1 DP voltammograms of PZB cultivars

The DP voltammograms of the PZB extract solutions from various origins, as shown in Fig. 3(a), were found to exhibit three to four peaks within the range of -0.2 to 1.4V. Notably, the DP voltammograms of the PZB derived from different regions exhibited significant variations. S1, S2 and S3, originating from geographically close areas (Tianshui City, Gansu Province), exhibited similar curve patterns, suggesting similar compositions. Conversely, S4, also sourced from Gansu Province, displayed a prominent anodic peak at approximately 0.6 V in its DP voltammograms, indicating the presence of distinct redox-active substances compared to its regional counterparts. Additionally, S6 and S7, obtained from Shanxi Province, demonstrated substantial disparities in voltammetry within the potential range of 0.2 V to 0.7 V. In contrast, S8 and S9, from Shandong Province, S10 from Hebei Province, and S11, S12, S13 and S14, from Sichuan Province, generally exhibited similar DP voltammograms.

3.2 Origin differentiation of PZB

To verify the potential of the DPV method for origin analysis, PCA and LDA were applied to reduce the dimensionality of the data and visualize the different categories. The results of the three-dimensional PCA score plot are shown in Fig. 3(b), in which the accumulated explained variance of the first three principal components is 93.3%. Although some aggregation trend was observed among same origin samples,

372 there was a significant overlap between different origin samples and, thus, the PCA
373 did not provide clear differentiations of the PZB origins.

374 Due to this limitation of the PCA, LDA was employed for further visualization.
375 In Fig. 3(c), in which the decision boundaries calculated from a two-dimensional LDA
376 space utilizing the KNN algorithm are presented, the plot clearly demonstrates distinct
377 differentiation among the PZB samples from different origins, with evident clusters of
378 PZB samples from the same origin. The DPV curve effectively captured the variations
379 and distinguishing characteristics of each origin, thereby facilitating comprehensive
380 analysis. Nevertheless, it is important to note the considerable overlap between
381 samples S4 and S9, which posed challenges for differentiation using LDA. Partial
382 overlap near the boundaries was also observed in samples S1, S2, S8 and S11,
383 resulting in misclassification. The scatter plot depicted in Fig. 3(c), resulting from the
384 LDA, visually illustrates the similarities between various samples, serving as a
385 foundation for further analysis. The underlying principle of the LDA's origin
386 differentiation capability lies in its ability to extract unique, differentiating
387 characteristics. By optimizing the linear combination of features, LDA maximizes
388 inter-group variance while minimizing intra-group variance, ensuring that samples
389 from the same origin are closely clustered while those from different origins are
390 clearly separated.

391 To further improve the accuracy of the PZB origin recognition model, we
392 evaluated the four different machine learning techniques, KNN, SVM, ANN and XGB.

Compared to LDA, these four algorithms were found to possess more flexible model structures and parameter settings, making them suitable for problem requirements. Additionally, they all exhibited proficiency in handling non-linear data and patterns, and typically demonstrated enhanced effectiveness in processing high-dimensional datasets. As summarized in Table 1 (the optimal hyperparameter setting details are provided in Table S5), All four models achieved 100% accuracy on the training set, but their performance on the test set showed significant differences. ANN achieved the highest recognition rate among the tested models, reaching 100%, followed by the recognition rates of SVM (92.8%), KNN (86.5%) and XGB (78.5%). KNN performed poorly due to the close proximity of certain PZB samples, as evident from the PCA and LDA analysis. The distance-based nature of the KNN algorithm does make sample distinction challenging (Feilat et al., 2019). The underperformance of XGB may be attributed to the sensitivity of tree-based ensemble models to feature partitioning and selection. An excess of features can amplify the risk of overfitting. Fig. 3(d) demonstrates the performance of the optimal model on the test set. The success of ANN in achieving the highest recognition rate underscored its capability in capturing complex interdependencies within the dataset, and demonstrating a discerning ability to discriminate between PZB origins. This improvement was possibly attributable to the self-adaptive feature representation learning ability, in which the useful features can be extracted from the raw data without feature engineering. Likewise, the proficiencies SVM can be attributed to their adeptness in

handling non-linear relationships and high-dimensional datasets.

The proposed DPV method exhibited a higher level of accuracy, reaching 100%, compared to the accuracies achieved by origin differentiation methods based on proton nuclear magnetic resonance (^{1}H NMR), at 86.8%, and near infrared (NIR), at 87.5% (Cui et al., 2023; Fan et al., 2021).

Identification of adulterated PZB

Though the origin differentiation model demonstrated good performance, the mixing of PZB from different origins can significantly reduce its accuracy. However, there is still few research monitoring adulteration behaviors that is a common phenomenon in PZB industry during PZB trading. To develop a reliable model for the identification of adulterated PZB, we further prepared samples containing various amounts of PZB from different origins. In evaluating the performances of the four different machine learning algorithms, we focused on the 50% fraud rate and the unadulterated samples and selected the optimal model based on the best binary classification performance. As shown in Table 1 (method detailed in Table S6), the KNN, XGB, SVM and ANN models all achieved excellent results, with their accuracy, precision, recall and AUC all exceeding 90%. The KNN model, in particular, achieved the highest accuracy rate of 97.9%, with its precision and recall close to 95% or even higher, and AUC reaching 0.980. These impressive metrics demonstrated that the KNN model was the most accurate and robust tool for the identification of adulteration in PZB samples.

To investigate the recognition threshold of the fraud model, data for samples with different rates of adulteration (20%, 35%, 50%, 65%, 80%) as well as that for the unadulterated samples were subsequently used to construct models. The optimal XGB model was used to analyze these datasets. In the results of this analysis, presented in Fig. 3(e), it is evident that the model's performance did not deteriorate significantly when the fraud rate decreased. The KNN model could effectively discriminate PZB samples with adulterants at even the 20% level with an accuracy of 87.4%, thereby demonstrating its robustness and reliability for this purpose.

3.3 Sensory evaluation of pungency intensity

Fig. 4(a) illustrates the sensory evaluations of the PZB samples sourced from different regions and indicates variations in pungency intensity based on origin. The PZB samples from various origins were subsequently ranked on the basis of their pungency intensities as follows: S1 (25.33 ± 3.91) ≥ S3 (24.69 ± 5.68) ≥ S13 (23.91 ± 4.68) ≥ S12 (21.64 ± 5.41) ≥ S2 (21.56 ± 3.80) ≥ S14 (20.09 ± 4.55) ≥ S11 (15.44 ± 6.25) ≥ S10 (12.31 ± 5.26) ≥ S4 (11.70 ± 2.81) ≥ S6 (11.61 ± 4.20) ≥ S7 (10.47 ± 4.19) ≥ S9 (9.38 ± 4.42) ≥ S5 (8.67 ± 4.59) ≥ S8 (7.30 ± 4.06). It is evident that these pungency intensity values vary considerably, representing different PZB grading. Specifically, PZB samples cultivated in the provinces of Gansu and Sichuan (S1, S2, S3, S12 and S13) generally exhibited higher pungency intensities, whereas the pungency intensities of samples from Hebei (S10), Shandong (S8 and S9) and Shaanxi (S6 and S7) were not as strong. Additionally, it was observed that S13

456 demonstrated similarities to S1, S3 and S12 in terms of high pungency intensity, while
457 S14, S2 and S11 shared a moderate pungency intensity.

458 In our previous study, we demonstrated a strong correlation between the total
459 alkylamide content of PZB and the peak current intensity around 1.0 V in the DP
460 voltammogram (Sun et al., 2020). In this work, combined with the analysis of the
461 DPV of PZB from different habitats shown in Fig. 3(a), most PZB samples with high
462 pungency intensity exhibited a pronounced peak intensity around 1.0 V. This is
463 consistent with previous findings that identified alkylamides as the primary pungent
464 compounds in PZB. However, some exceptions were observed. For instance, PZB
465 sample S7 possessed a relatively high alkylamide content but low pungency intensity,
466 while S12, despite having a relatively low alkylamide content, exhibited high
467 pungency intensity. These exceptions suggest the presence of other constituents with
468 an influence on the pungency intensity of PZB, in addition to alkylamides.

469 **3.4 Prediction of PZB pungency intensity**

470 To assess the pungency intensity of PZB, the performances of the four distinct
471 learning algorithms were assessed using R^2 and RMSE on their training, validation
472 and test datasets. In Table 1, the optimal results achieved by each model are
473 summarized, while the hyperparameters used by each model are provided in Table S7.

474 Among the tested four algorithms, the KNN algorithm yielded the highest
475 training R^2 value, at 1.00, while the SVM algorithm exhibited the lowest value, at
476 0.952. The cross-validation R^2 values ranged from 0.752 to 0.896, indicating

variations in performance across the algorithms. Notably, based on the difference between R^2 and RMSE in the training and cross validation sets (ΔR^2=0.048 and ΔRMSE=0.98, respectively), the ANN algorithm demonstrated minimal performance disparity between the two sets, suggesting no significant overfitting issues. Conversely, the performance degradation of the KNN algorithm was more pronounced, and the other two algorithms both exhibited a poor performance with a significant decline compared to the training set, which indicated clear overfitting concerns. This issue could, however, be potentially mitigated by expanding the dataset (Greener et al., 2022b).

In evaluating prediction performance on the test dataset, all algorithms achieved R^2 ranging from 0.743 to 0.918. The ANN algorithm exhibited the highest R^2 at 0.918, while the XGB algorithm demonstrated the lowest performance with an R^2 of 0.743. These test dataset results align with the cross-validation findings. Consequently, the ANN algorithm emerged as the most effective model for evaluating PZB pungency intensity. Fig. 4(c) showcases scatter plots that illustrate the regression results of the best-performing model for both training and testing. The x-axis represents the actual values, while the y-axis represents the predicted values, and a scatter distribution closely aligned with the diagonal line is an indication of superior model performance. The optimal ANN model was achieved with hyperparameters set to num_layers of 4 and hidden size of 128. This restraint of ANN model architecture curbed excessive complexity and the potential for overfitting. Thus, by incorporating dropout and

regularization strategies, the ANN algorithm effectively prevented the network from becoming overly sensitive to noise in the training data.

On the other hand, the performance of the pungency intensity prediction model was shown to be limited since the sensory evaluation data fluctuated significantly. Notwithstanding, the DPV-ANN model proposed in this present work is demonstrably superior to a prediction model based on NIR combined with partial least squares (Fan et al., 2021), and presented a higher accuracy (0.918 vs. 0.822, respectively). Compared to the usage of electrochemical method alone (Dejmkova et al., 2018; Hao et al., 2023), the combination of electrochemical methods with machine learning algorithms reduces the influence of interfering substances on electrochemical detection accuracy, eliminating intricate sample pretreatment or electrode modification process. This not only results in cost savings but also enhances detection efficiency. The performance disparities among different pungency intensity detection methods are listed in Table S8.

To investigate the impact of individual DP voltammetric features on model output, the feature importance of the optimal model was analyzed, the results of which are presented in Fig. 4(d). Brighter colors indicate the greater contributions of corresponding points to the model. Two relatively bright bands are evident at 0.34-0.52 V and 1.0-1.2 V, and it has been previously reported that the peak potentials of polyphenols and alkylamides in PZB fall within these ranges (Sun et al., 2020a), which suggests that these two substances are closely related to pungency intensity in

519 PZB. To further verify the impact of features attributed to polyphenol on the
520 pungency intensity evaluation model, these features were excluded and the model was
521 retrained with the optimal hyperparameters. The performance of the feature ablation
522 model on the test set decreased from R^2=0.918 to R^2=0.831, a decline that clearly
523 demonstrated the impact of polyphenol components on the pungency intensity of PZB.
524 Removal of these correlated features diminished the ability of the model to capture
525 the intricate interaction between polyphenols and pungency, resulting in reduced
526 predictive accuracy.

527 **3.5 Mechanism of pungency intensity detection via DPV assay**

528 To elucidate the mechanism through which DP voltametric signals are able to
529 rapidly quantify the pungency intensity of PZB, the relationship between the
530 voltametric characteristics of primary pungent substances, namely hydroxyl-α, β and
531 γ- sanshool (α, β, γ- SOH) and pungency intensities were analyzed. As shown in Figs.
532 5(a) to (c), the anodic peak potential of the three SOHs were measured as 0.93, 0.95
533 and 0.92V, respectively. The peak intensity (I_p) of each SOH exhibited a good linear
534 relationship with its concentration gradient. In addition, a linear regression was run to
535 quantify the relationship between the peak potential (E_p), I_p and peak area (A_p) of the
536 SOHs at different concentrations, and the SPU of SOH. The fitting equation was as
537 follows:

538 $SPU = -630.75.E_p + 662.60\,I_p + 694.86A_p + 737.40$ with $R^2 = 0.952$.

539 The results suggested that the pungency intensity of SOH is negatively correlated

with E_p, yet positively related with I_p. It has been well documented that the numbing sensation of SOH is primarily attributed to the stimulation of the transient receptor potential vanilloid 1 (TRPV1) and TRP ankyrin 1 (TRPA1), and it has been demonstrated that α-SOH acts on TRPA1 and TRPV1 through either covalent or non-covalent interactions with specific cysteine residues (Riera et al., 2009; Xiao et al., 2021). Since both TRPV1 and TRPA1 are redox biosensors and their stimulation is closely related to redox status (Luo et al., 2022), it can be speculated that SOH with lower oxidation potential (i.e., lower E_p value) will be preferably oxidized, correspondingly facilitating its interact with TRPV1 or TRPA1. This explains why the DP voltammogram was able to distinguish between the pungency intensities of the different SOHs.

In addition to hydroxyl-sanshools, the contributions of phenolic components to the total pungency intensity of PZB were observed via the feature importance analysis described in section 3.5. To interpret these phenomena, the DPV features of the purified phenol standard (i.e. quercetin, a representative of PZB polyphenols) and IPF were analyzed. The chromatography of the IPF from S14 and its composition are depicted in Fig. S1, in which it is evident that the IPF contained no alkylamides.

Two anodic peaks appeared at 0.26-0.43 V and 0.96-1.2 V from the quercetin DPV (Fig. 5(d)), while three anodic peaks were observed at around 0.3, 0.6 and 1.1 V from IPF's voltammogram (Fig.5(e)), suggesting the presence of other polyphenols. With the combination of IPF and α-SOH, the peak intensities at 0.26-0.43 and 0.42-

561 0.71 V decreased sharply. In contrast, the peak at 1.1 V was integrated with the
562 characteristic peak of α-SOH, exhibiting a significant increase in peak intensity and a
563 positive shift of E_p from α-SOH. The DP voltammogram of the IPF/α-SOH
564 combination was basically consistent with that of PZB samples such as S14 (Fig. 5(f)),
565 suggesting that the DPV signal interaction between polyphenol and SOH are well
566 reflected in the pungency intensity prediction. Furthermore, it has been clarified that
567 some polyphenols activate TRPV1 or TRPA1 to produce an astringent taste, which is
568 also a trigeminal sense (Schöbel et al., 2014). It is evident that the sense overlap
569 between polyphenols and SOHs from PZB was fully reflected via DPV.

570 These findings demonstrate that DPV combined with machine learning
571 algorithms is able to capture the redox characteristics of polyphenols and SOH in PZB,
572 as well as to simulate the interaction between the two types of ingredients, thereby
573 achieving an accurate measurement of pungency intensity.

574 **4 Conclusions**

575 The development of a rapid and reliable method with which to assess the quality
576 of PZB is vital to the economic and reputational integrity of this popular spice
577 condiment. In this study, we combined electrochemical analysis with machine
578 learning methods to establish a rapid approach for the detection of PZB geographical
579 authenticity and pungency intensity in quality monitoring during commercial
580 transactions, and in grading during deep processing. Our research achieved a 100%
581 accuracy in distinguishing the origin of PZB, as well as 97.9% accuracy in the

identification of PZB adulteration. Furthermore, the KNN machine learning method successfully discriminated between pure PZB samples and adulterated ones, with an accuracy of 87.4% even in the diminished presence of 20% adulteration. In a parallel assay, the neural network achieved the best performance in the prediction of pungency intensity (R^2 = 0.918). In addition to alkylamides, it was found that polyphenols in PZB may also contribute to overall pungency intensity, adding a new dimension to our understanding of the factors influencing PZB's sensory attributes. Our study, thus, underscores the potential of combining electrochemistry with machine learning methods to provide a swift, reliable and innovative approach for the authenticating and grading of PZB, and its findings have beneficial implications for the food industry.

Acknowledgments

Thanks for the Fund of Key R&D plan of Shandong Province (2022TZXD0030) and the key Program Fund for China National Institute of Standardization (562022Y-9417)

References

Abu Alfeilat, H. A., Hassanat, A. B. A., Lasassmeh, O., Tarawneh, A. S., Alhasanat, M. B., Eyal Salman, H. S., & Prasath, V. B. S. (2019). Effects of Distance Measure Choice on K-Nearest Neighbor Classifier Performance: A Review. *Big Data*, *7*(4), 221–248. https://doi.org/10.1089/big.2018.0175

Anowar, F., Sadaoui, S., & Selim, B. (2021). Conceptual and empirical comparison of dimensionality reduction algorithms (PCA, KPCA, LDA, MDS, SVD, LLE,

603 ISOMAP, LE, ICA, t-SNE). *Computer Science Review*, *40*, 100378.
604 https://doi.org/10.1016/j.cosrev.2021.100378
605 Artaria, C., Maramaldi, G., Bonfigli, A., Rigano, L., & Appendino, G. (2011). Lifting
606 properties of the alkamide fraction from the fruit husks of Zanthoxylum
607 bungeanum: Lifting activity of Z. bungeanum fraction. *International Journal*
608 *of Cosmetic Science*, *33*(4), 328–333. https://doi.org/10.1111/j.1468-
609 2494.2010.00629.x
610 Barnes, R. J., Dhanoa, M. S., & Lister, S. J. (1989). Standard Normal Variate
611 Transformation and De-Trending of Near-Infrared Diffuse Reflectance Spectra.
612 *Applied Spectroscopy*, *43*(5), 772–777.
613 https://doi.org/10.1366/0003702894202201
614 Cui, C., Xia, M., Wei, Z., Chen, J., Peng, C., Cai, H., Jin, L., & Hou, R. (2023). 1H
615 NMR-based metabolomic approach combined with machine learning
616 algorithm to distinguish the geographic origin of huajiao (Zanthoxylum
617 bungeanum Maxim.). *Food Control*, *145*, 109476.
618 https://doi.org/10.1016/j.foodcont.2022.109476
619 Dejmkova, H., Morozova, K., & Scampicchio, M. (2018). Estimation of Scoville
620 index of hot chili peppers using flow injection analysis with electrochemical
621 detection. *Journal of Electroanalytical Chemistry*, *821*, 82–86.
622 https://doi.org/10.1016/j.jelechem.2018.01.056
623 Erickson, N., Mueller, J., Shirkov, A., Zhang, H., Larroy, P., Li, M., & Smola, A.

(2020). *AutoGluon-Tabular: Robust and Accurate AutoML for Structured Data* (arXiv:2003.06505). arXiv. http://arxiv.org/abs/2003.06505

Fan, L., Zhang, C., Zhao, R., He, L., Fan, W., Wu, C., & Huang, Y. (2021). Rapid and Nondestructive Determination of origin, volatile oil, sanshoamides and crack rate in the 'Sichuan Pepper' Based on a Novel Portable Near Infrared Spectrometer. *Journal of Food Composition and Analysis*, *101*, 103942. https://doi.org/10.1016/j.jfca.2021.103942

Feng, X., Huang, P., Duan, P., Wang, H., & Kan, J. (2023). Dynamic Zanthoxylum pungency characteristics and their correlation with sanshool composition and chemical structure. *Food Chemistry*, *407*, 135138. https://doi.org/10.1016/j.foodchem.2022.135138

Feng, X., Wang, H., Wang, Z., Huang, P., & Kan, J. (2022). Discrimination and characterization of the volatile organic compounds in eight kinds of huajiao with geographical indication of China using electronic nose, HS-GC-IMS and HS-SPME-GC–MS. *Food Chemistry*, *375*, 131671. https://doi.org/10.1016/j.foodchem.2021.131671

GB/T 38495. 2020. Sensory analysis—Sensory evaluation of Chinese pepper pungency intensity—Scoville index determination method.

Ghoreishi, S. M., Behpour, M., Mousavi, S., Khoobi, A., & Ghoreishi, F. S. (2014). Simultaneous electrochemical determination of dopamine, ascorbic acid and uric acid in the presence of sodium dodecyl sulphate using a multi-walled

carbon nanotube modified carbon paste electrode. *RSC Advances*, *4*(72), 37979–37984. https://doi.org/10.1039/C4RA04919E

Greener, J. G., Kandathil, S. M., Moffat, L., & Jones, D. T. (2022a). A guide to machine learning for biologists. *Nature Reviews Molecular Cell Biology*, *23*(1), Article 1. https://doi.org/10.1038/s41580-021-00407-0

Greener, J. G., Kandathil, S. M., Moffat, L., & Jones, D. T. (2022b). A guide to machine learning for biologists. *Nature Reviews Molecular Cell Biology*, *23*(1), 40–55. https://doi.org/10.1038/s41580-021-00407-0

Hao, M., Li, Z., Huang, X., Wang, Y., Wei, X., Zou, X., Shi, J., Huang, Z., Yin, L., Gao, L., Li, Y., Holmes, M., & Elrasheid Tahir, H. (2023). A cell-based electrochemical taste sensor for detection of Hydroxy-α-sanshool. *Food Chemistry*, *418*, 135941. https://doi.org/10.1016/j.foodchem.2023.135941

Hu, L., Xu, Z., Fan, R., Wang, G., Wang, F., Qin, X., Yan, L., Ji, X., Meng, M., Sim, S., Chen, W., Hao, C., Wang, Q., Zhu, H., Zhu, S., Xu, P., Zhao, H., Lindsey, K., Daniell, H., … Jin, S. (2023). The complex genome and adaptive evolution of polyploid Chinese pepper (Zanthoxylum armatum and Zanthoxylum bungeanum). *Plant Biotechnology Journal*, *21*(1), 78–96. https://doi.org/10.1111/pbi.13926

Ke, J., Qu, Y., Li, S., Shen, G., Chen, A., Luo, Q., Liu, X., Wu, H., Li, M., Pu, B., Ye, M., & Zhang, Z. (2018). Application of HPLC fingerprint based on acid amide components in Chinese prickly ash (Zanthoxylum). *Industrial Crops and*

Products, *119*, 267–276. https://doi.org/10.1016/j.indcrop.2018.04.018

Kumar, V., Kumar, S., Singh, B., & Kumar, N. (2014). Quantitative and structural analysis of amides and lignans in Zanthoxylum armatum by UPLC-DAD-ESI-QTOF–MS/MS. *Journal of Pharmaceutical and Biomedical Analysis*, *94*, 23–29. https://doi.org/10.1016/j.jpba.2014.01.028

Li, W., Wu, Y., Liu, Y., Tang, Y., Che, Z., & Wu, T. (2020). Chemical profiles and screening of potential α-glucosidase inhibitors from Sichuan pepper using ultra-filtration combined with UHPLC-Q-TOF. *Industrial Crops and Products*, *143*, 111874. https://doi.org/10.1016/j.indcrop.2019.111874

Luo, J., Ke, J., Hou, X., Li, S., Luo, Q., Wu, H., Shen, G., & Zhang, Z. (2022). Composition, structure and flavor mechanism of numbing substances in Chinese prickly ash in the genus Zanthoxylum: A review. *Food Chemistry*, *373*, 131454. https://doi.org/10.1016/j.foodchem.2021.131454

Marx, Í. M. G. (2023). Emerging Trends of Electrochemical Sensors in Food Analysis. *Electrochem*, *4*(1), Article 1. https://doi.org/10.3390/electrochem4010004

Oliveri, P., Malegori, C., Simonetti, R., & Casale, M. (2019). The impact of signal pre-processing on the final interpretation of analytical outcomes – A tutorial. *Analytica Chimica Acta*, *1058*, 9–17. https://doi.org/10.1016/j.aca.2018.10.055

Peris-Díaz, M. D., & Krężel, A. (2021). A guide to good practice in chemometric methods for vibrational spectroscopy, electrochemistry, and hyphenated mass spectrometry. *TrAC Trends in Analytical Chemistry*, *135*, 116157.

https://doi.org/10.1016/j.trac.2020.116157

Press, W. H., & Teukolsky, S. A. (1990). Savitzky-Golay Smoothing Filters. *Computers in Physics*, *4*(6), 669. https://doi.org/10.1063/1.4822961

Raju, V. N. G., Lakshmi, K. P., Jain, V. M., Kalidindi, A., & Padma, V. (2020). Study the Influence of Normalization/Transformation process on the Accuracy of Supervised Classification. *2020 Third International Conference on Smart Systems and Inventive Technology (ICSSIT)*, 729–735. https://doi.org/10.1109/ICSSIT48917.2020.9214160

Riera, C., Menozzi-Smarrito, C., Affolter, M., Michlig, S., Munari, C., Robert, F., Vogel, H., Simon, S., & Le Coutre, J. (2009). Compounds from Sichuan and Melegueta peppers activate, covalently and non-covalently, TRPA1 and TRPV1 channels. *British Journal of Pharmacology*, *157*(8), 1398–1409. https://doi.org/10.1111/j.1476-5381.2009.00307.x

Schöbel, N., Radtke, D., Kyereme, J., Wollmann, N., Cichy, A., Obst, K., Kallweit, K., Kletke, O., Minovi, A., Dazert, S., Wetzel, C. H., Vogt-Eisele, A., Gisselmann, G., Ley, J. P., Bartoshuk, L. M., Spehr, J., Hofmann, T., & Hatt, H. (2014). Astringency Is a Trigeminal Sensation That Involves the Activation of G Protein–Coupled Signaling by Phenolic Compounds. *Chemical Senses*, *39*(6), 471–487. https://doi.org/10.1093/chemse/bju014

Shi, J., Wang, Y., Li, Z., Huang, X., Shen, T., & Zou, X. (2021). Simultaneous and nondestructive diagnostics of nitrogen/magnesium/potassium-deficient

cucumber leaf based on chlorophyll density distribution features. *Biosystems Engineering*, *212*, 458–467. https://doi.org/10.1016/j.biosystemseng.2021.11.001

Sugai, E., Morimitsu, Y., Iwasaki, Y., Morita, A., Watanabe, T., & Kubota, K. (2005). Pungent Qualities of Sanshool-Related Compounds Evaluated by a Sensory Test and Activation of Rat TRPV1. *Bioscience, Biotechnology, and Biochemistry*, *69*(10), 1951–1957. https://doi.org/10.1271/bbb.69.1951

Sun, X., Zhang, D., Zhao, L., Shi, B., Xiao, J., Liu, X., Zekruman, M., Hu, Y., Ngouana, A., Shi, J., & Zou, X. (2020). Antagonistic interaction of phenols and alkaloids in Sichuan pepper (Zanthoxylum bungeanum) pericarp. *Industrial Crops and Products*, *152*, 112551. https://doi.org/10.1016/j.indcrop.2020.112551

Sun, X., Zhang, D., Zhao, L., Shi, B., Xiao, J., Shi, J., & Zou, X. (2020). Development of differential pulse voltammetric method for rapid quantification of total hydroxyl-sanshools in Sichuan Pepper. *LWT*, *130*, 109640. https://doi.org/10.1016/j.lwt.2020.109640

Valian, M., Khoobi, A., & Salavati-Niasari, M. (2020). Green synthesis and characterization of DyMnO3-ZnO ceramic nanocomposites for the electrochemical ultratrace detection of atenolol. *Materials Science and Engineering: C*, *111*, 110854. https://doi.org/10.1016/j.msec.2020.110854

Vilas-Boas, Â., Valderrama, P., Fontes, N., Geraldo, D., & Bento, F. (2019).

729 Evaluation of total polyphenol content of wines by means of voltammetric
730 techniques: Cyclic voltammetry vs differential pulse voltammetry. *Food*
731 *Chemistry*, *276*, 719–725. https://doi.org/10.1016/j.foodchem.2018.10.078
732 Xiao, S., Song, P., Bu, F., Pang, G., Zhou, A., Zhang, Y., & Xie, J. (2021). The
733 investigation of detection and sensing mechanism of spicy substance based on
734 human TRPV1 channel protein-cell membrane biosensor. *Biosensors and*
735 *Bioelectronics*, *172*, 112779. https://doi.org/10.1016/j.bios.2020.112779
736 Yang, L., Gao, H., Meng, L., Fu, X., Du, X., Wu, D., & Huang, L. (2021).
737 Nondestructive measurement of pectin polysaccharides using hyperspectral
738 imaging in mulberry fruit. *Food Chemistry*, *334*, 127614.
739 https://doi.org/10.1016/j.foodchem.2020.127614
740 Zhang, D., Fan, Y., Sun, X., Wei, X., Lin, Z., Zhang, X., Shi, J., Battino, M., Gong, Y.,
741 Shi, B., & Zou, X. (2023). SERS determination of hydroxy-α-sanshool in
742 spicy hotpot seasoning: The strategy to restrain the interference of capsaicin
743 and its mechanism. *Food Chemistry*, *413*, 135644.
744 https://doi.org/10.1016/j.foodchem.2023.135644
745 Zhang, D., Sun, X., Battino, M., Wei, X., Shi, J., Zhao, L., Liu, S., Xiao, J., Shi, B., &
746 Zou, X. (2021). A comparative overview on chili pepper (capsicum genus) and
747 sichuan pepper (zanthoxylum genus): From pungent spices to pharma-foods.
748 *Trends in Food Science & Technology*, *117*, 148–162.
749 https://doi.org/10.1016/j.tifs.2021.03.004

Zhang, L., Zhao, L., Wang, H., Shi, B., Liu, L., & Chen, Z. (2019). The relationship between alkylamide compound content and pungency intensity of *Zanthoxylum bungeanum* based on sensory evaluation and ultra-performance liquid chromatography-mass spectrometry/ mass spectrometry (UPLC-MS/MS) analysis: Alkylamide compound content and pungency intensity of *Zanthoxylum bungeanum*. *Journal of the Science of Food and Agriculture*, *99*(4), 1475–1483. https://doi.org/10.1002/jsfa.9319

Zhang, L.-L., Xu, S.-S., Shi, B.-L., Wang, H.-Y., Liu, L.-Y., Zhong, K., Zhao, L., & Chen, Z.-X. (2018). Evaluation of the pungency intensity and time-related aspects of Chinese *Zanthoxylum bungeanum* based on human sensation. *Journal of Sensory Studies*, *33*(6), e12465. https://doi.org/10.1111/joss.12465

Table and Figure Captions

Table 1. Performances of three kinds of models: PZB origin differentiation models evaluated with dataset 1, in which accuracy (Acc) and log loss (LL) are reported; as well as PZB adulteration identification models evaluated with the dataset 2 in which Acc, Pre, recall (Rec) and Area Under Curve (AUC) are reported; PZB pungency intensity prediction models evaluated with dataset 3, in which R-Squared (R2) reflects the degree of fit between the estimated value of the trend line and the corresponding actual data and root mean square error (RMSE).

Fig.1 Appearance and origin information of PZB samples. The provinces from which the PZB samples came are marked on the China map, and the exact locations of the

771 samples are marked on a locally enlarged map of the specific provinces.

772 Fig. 2 Dataset establishment.

773 Fig. 3 (a) Average DP voltammograms of PZB from different origins (S1-S4 from
774 Gansu, S5 from Shanxi, S6-S7 from Shaanxi, S8-S9 from Shandong, S10-S14 from
775 Sichuan); (b) PCA scores plot of the all DP voltammograms (210 samples, 210 × 400
776 variables) (93.3% total variance); (c) Computed decision boundary of PZB origin
777 differentiation based on KNN model; (d) Confusion matrix in test set of the best PZB
778 origin analysis model; (e) Best model adulteration identification accuracy at different
779 rates of PZB adulteration.

780 Fig. 4 (a) Pungency intensities of PZB grown in different origins (color of box
781 diagram indicates the province in which the sample was cultivated, and ◊ represents
782 outlier point); (b) Scale and description semantics for PZB pungency intensity; (c)
783 Scatter plots of measured and predicted values of the best PZB pungency intensity
784 prediction model; (d) Contribution of each feature used to build the PZB pungency
785 intensity prediction model.

786 Fig. 5. DP voltammograms (a-c) α, β and γ -SOH with different concentration
787 gradients (10, 20, 30, 40, 50 g/L); (d) quercetin (30 g/L); (e) IPF (30 g/L), α-SOH (30
788 g/L) and mixtures of IPF and α-SOH; (f) PZB extract sample (S14)

Table 1. Performances of three kinds of models: PZB origin differentiation models evaluated with dataset 1, in which accuracy (Acc) and log loss (LL) are reported; as well as PZB adulteration identification models evaluated with the dataset 2 in which Acc, Pre, recall (Rec) and Area Under Curve (AUC) are reported; PZB pungency intensity prediction models evaluated with dataset 3, in which R-Squared (R^2) reflects the degree of fit between the estimated value of the trend line and the corresponding actual data and root mean square error (RMSE).

	origin differentiation models						adulteration identification models												pungency intensity prediction models					
method	Acc			LL			Acc			Pre			Rec			AUC			R^2			RMSE		
	train	cv	test	train	cv	test	train	cv	test	train	cv	test	train	cv	test	train	cv	test	train	cv	test	train	cv	test
KNN	**100**	87.5	86.5	**0.000**	1.000	1.417	**100**	96.4	**97.9**	**100.0**	**98.0**	**95.9**	**100**	94.9	**100**	**1.00**	0.964	**0.98**	**1.00**	0.826	0.867	**0.00**	4.93	4.20
ANN	**100**	**98.2**	**100**	0.003	**0.116**	**0.019**	97.9	**97.9**	95.8	96.0	96.0	92.0	**100**	**100**	**100**	0.979	**0.979**	0.96	0.944	**0.896**	**0.918**	2.79	**3.77**	**3.29**
XGB	**100**	84.5	78.5	0.325	0.820	0.950	97.9	95.8	95.8	96.0	94.0	92.0	**100**	97.9	**100**	0.958	0.958	0.96	0.982	0.752	0.743	1.61	5.87	5.83
SVM	**100**	92.9	92.8	0.739	0.835	0.939	97.9	**97.9**	95.8	96.0	96.0	92.0	**100**	**100**	**100**	0.958	**0.979**	0.96	0.952	0.826	0.867	2.59	4.93	4.20

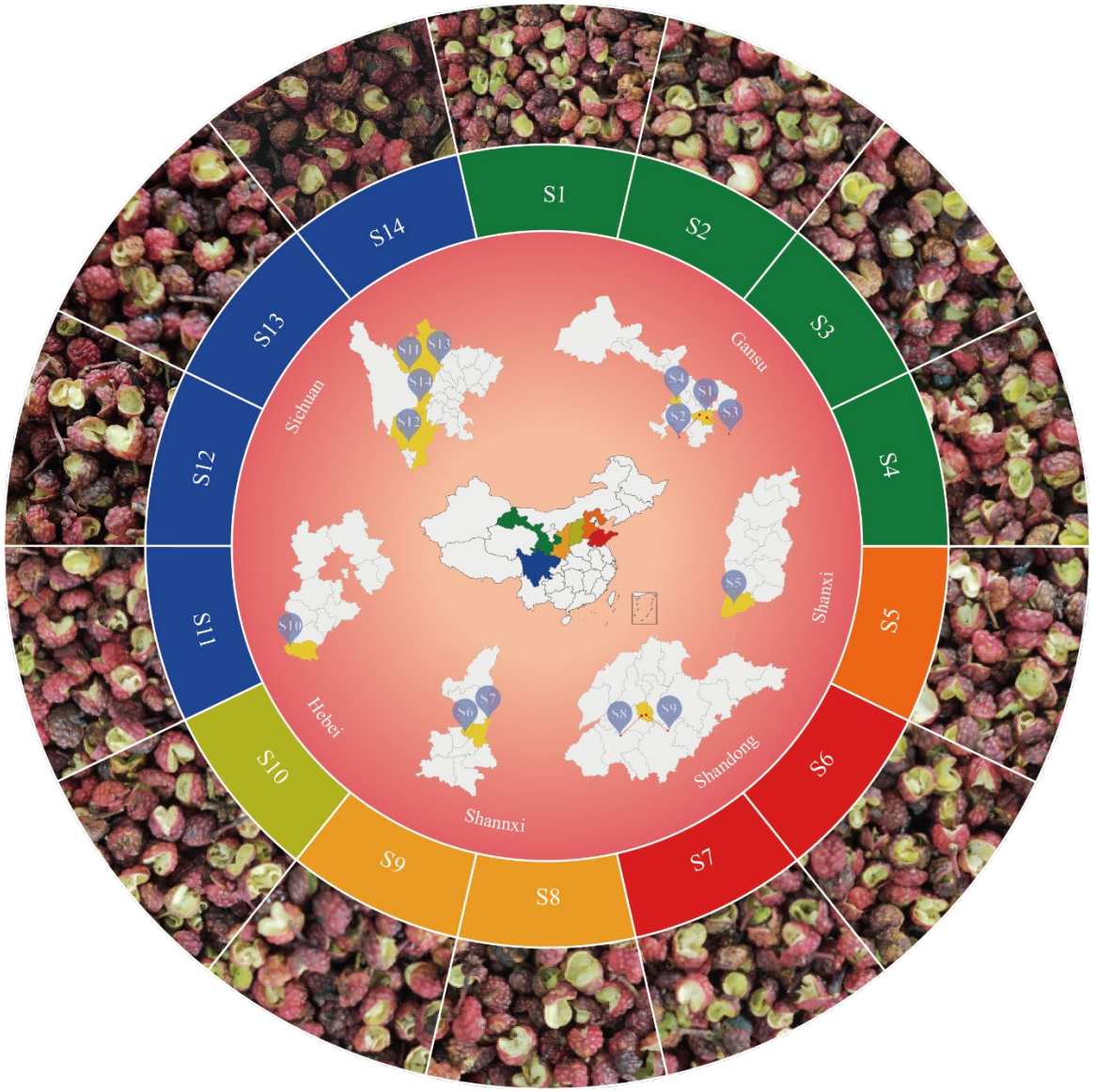

Fig.1. Appearance and origin information of PZB samples. The provinces from which the PZB samples came are marked on the China map, and the exact locations of the samples are marked on a locally enlarged map of the specific provinces.

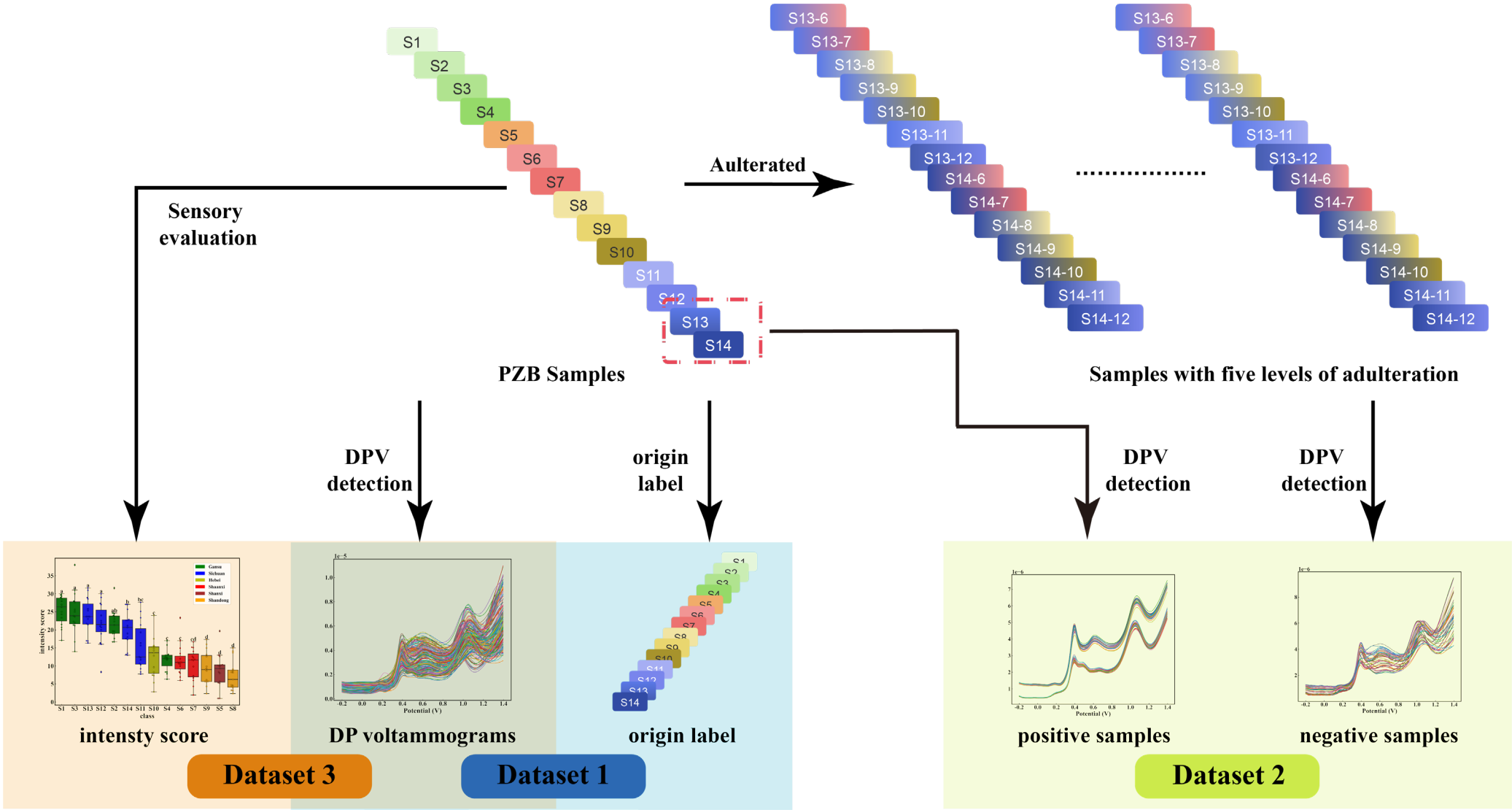

Fig.2. Dataset establishment.

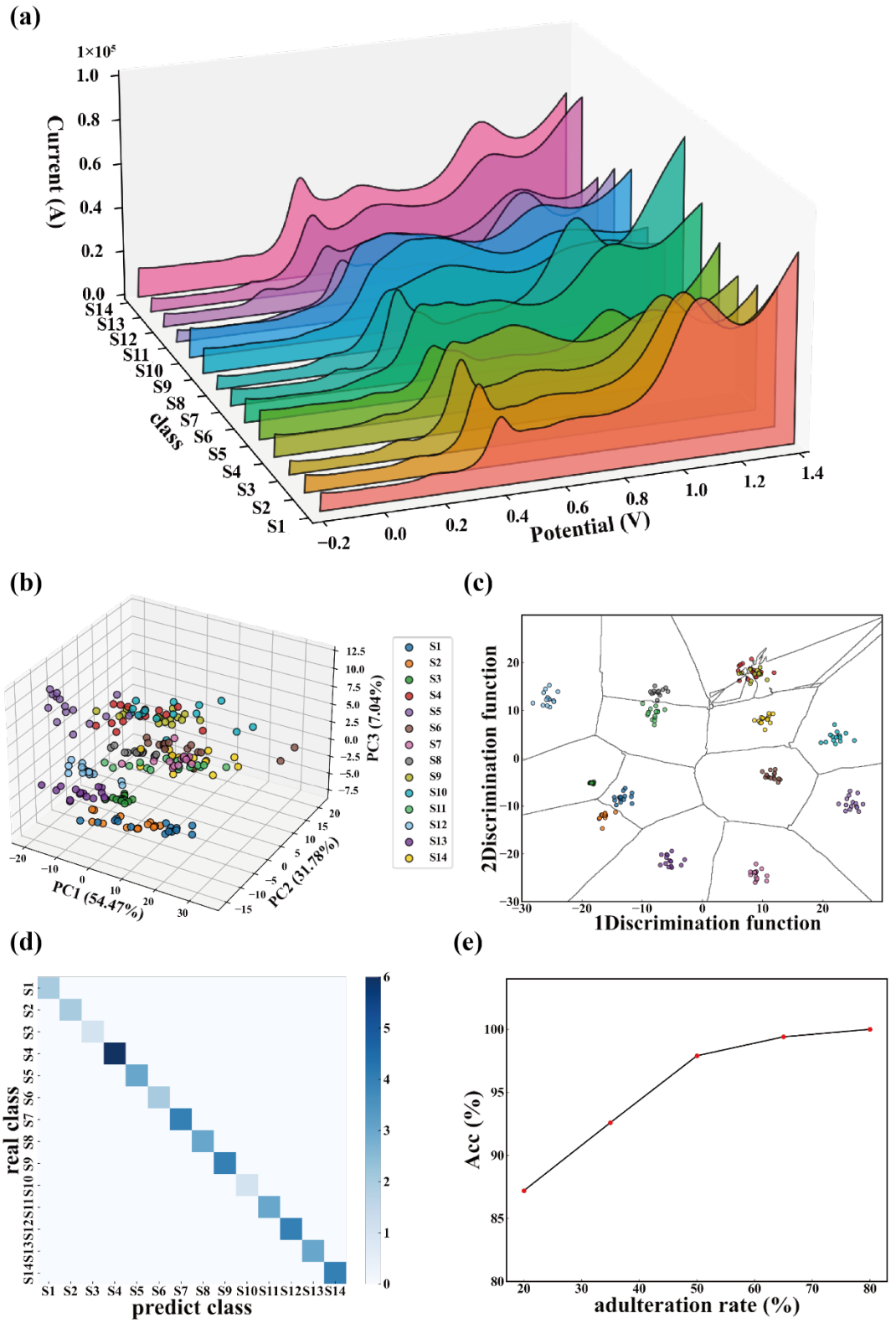

Fig.3. (a) Average DP voltammograms of PZB from different origins (S1-S4 from Gansu, S5 from Shanxi, S6-S7 from Shaanxi, S8-S9 from Shandong, S10-S14 from Sichuan); (b) PCA scores plot of the all DP voltammograms (210 samples, 210 × 400 variables) (93.3% total variance); (c) Computed decision boundary of PZB origin differentiation based on KNN model; (d) Confusion matrix in test set of the best PZB origin analysis model; (e) Best model adulteration identification accuracy at different rates of PZB adulteration.

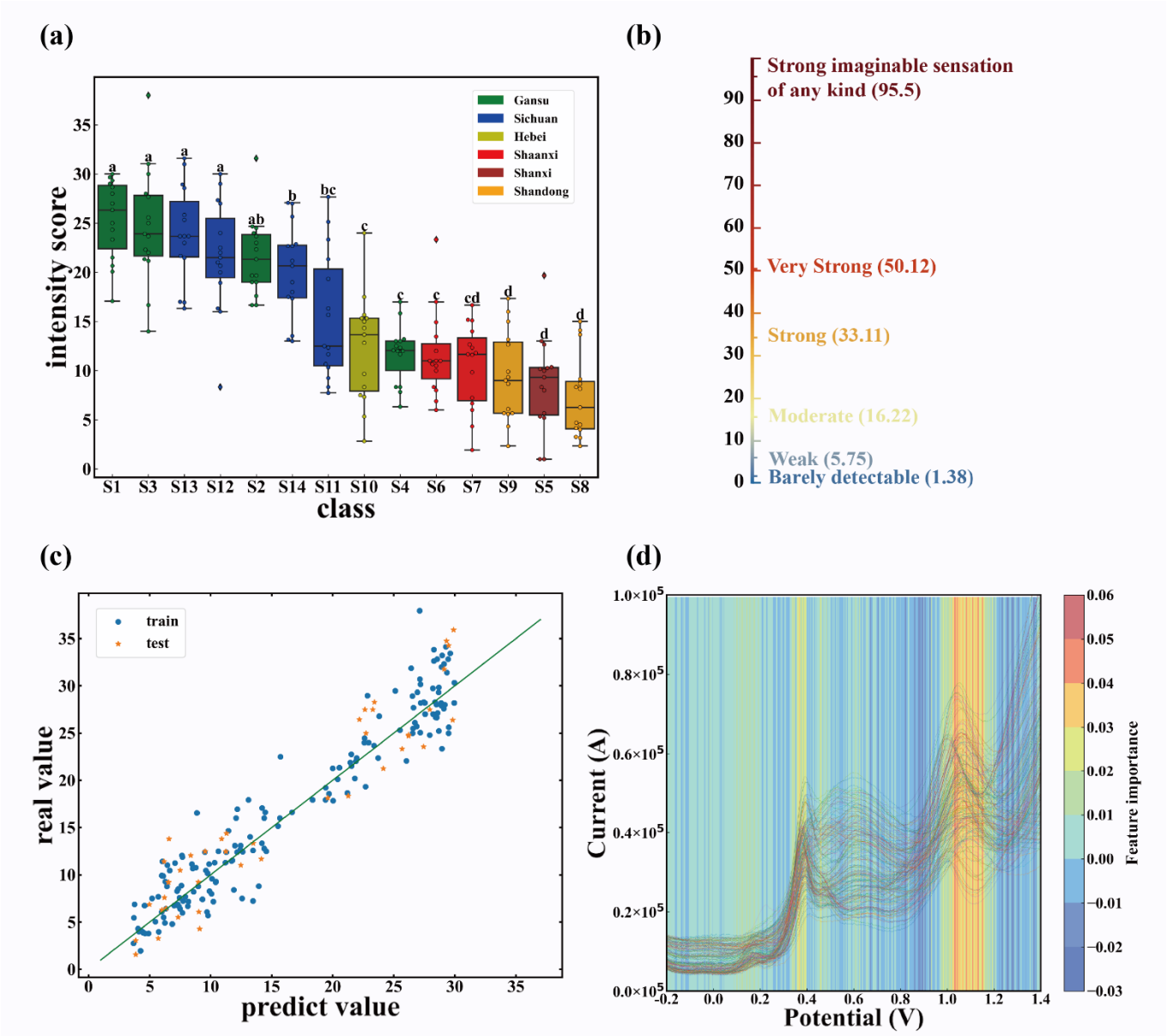

Fig.4. (a) Pungency intensities of PZB grown in different origins (color of box diagram indicates the province in which the sample was cultivated, and ◊ represents outlier point); (b) Scale and description semantics for PZB pungency intensity; (c) Scatter plots of measured and predicted values of the best PZB pungency intensity prediction model; (d) Contribution of each feature used to build the PZB pungency intensity prediction model.

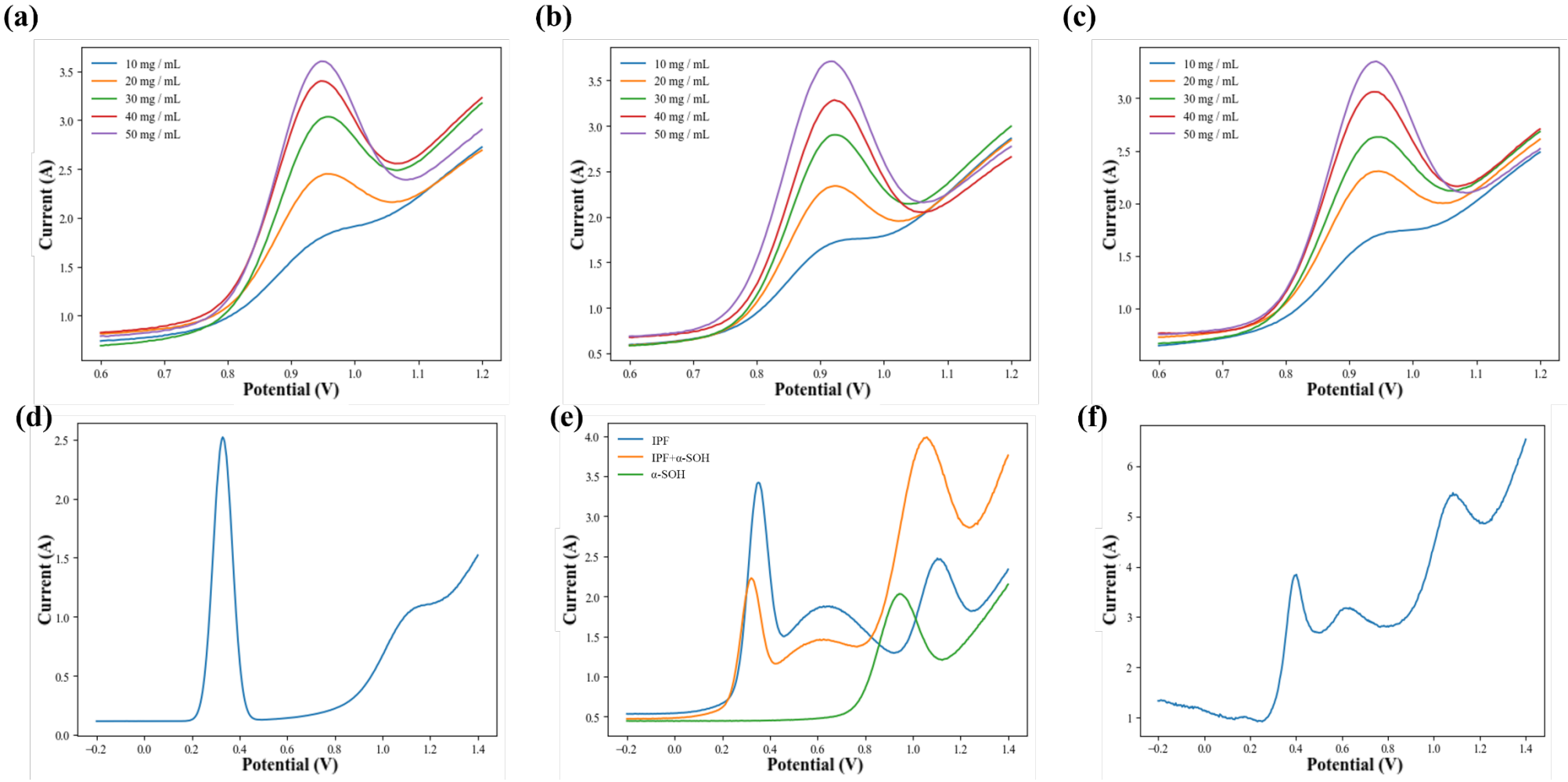

Fig.5. DP voltammograms (a-c) α, β and γ -SOH with different concentration gradients (10, 20, 30, 40, 50 g/L); (d) quercetin (30 g/L); (e) IPF (30 g/L), α-SOH (30 g/L) and mixtures of IPF and α-SOH; (f) PZB extract sample (S14).